LASER TWEEZERS

A thesis submitted in partial fulfillment of the requirement
for the degree of Bachelor of Science with Honors in
Physics from the College of William and Mary in Virginia,

by

Paul Lloyd Larsen

Accepted for _____
(Honors, High Honors, or Highest Honors)

_____
Director

_____

_____

_____

Williamsburg, Virginia
April 1999

Luke Skywalker: “Why are we still moving towards it?”

Han Solo: “We’re caught in a tractor beam; it’s pulling us in.”

-*Star Wars: A New Hope*[1]

Contents

I. Abstract

In this paper we explore the theory and practice of laser tweezers. We examine the forces involved in laser tweezers in order to understand how trapping occurs. We look at two simplified cases—a totally transmitting sphere and a totally reflecting sphere. We also propose a geometrical model that gives a value for the maximum trapping force on a transmitting sphere.

In the experimental section, we describe the construction of our laser tweezer. We report evidence of trapping, and calibrate the trap strength with viscous forces.

II. Introduction

Laser tweezers are the next best thing to a tractor beam. Since 1970, scientists have used single beam traps to manipulate objects ranging from dielectric spheres[2] to sperm cells[3] to DNA.[4] Laser tweezers have opened exciting avenues of research, especially in cell biology.

Laser tweezers operate through the radiation pressure of light. Light carries momentum, equal to h/λ per photon, where h is Planck's constant and λ is the wavelength of the light. When light hits an object and is reflected or refracted, the outgoing light has a different momentum than the incident light. Thus there is a change in momentum of the light, Δp_{light}. For momentum to be conserved, there must be an equal and opposite change in the momentum of the object, so $\Delta p_{\text{obj}} = -\Delta p_{\text{light}}$.

In the seventeenth century, Johannes Kepler appealed to radiation pressure to explain why a comet's tail points away from the sun.[5] Due to the diminutive size of radiation forces, however, practical applications of radiation forces only came with the invention of lasers. A. Ashkin first demonstrated trapping with radiation forces in 1970 using a 1 W cw argon laser and latex spheres about 1 μm in diameter.[2] This work paved the way for atom trapping,[6,7] and the realization of a Bose-Einstein condensate.

The earliest optical traps used multiple beams[8] or an opposing force (such as gravity[9]) to construct a stable trap. In 1986, however, A. Ashkin, J.M. Dziedzic, J.E. Bjorkholm, and S. Chu constructed a three-dimensional trap using a single laser beam.[10] Recent attention has turned to applications of the single beam laser trap in cell and microbiology.[11,12,13] In these applications, and our experiment, the sample is suspended in liquid, so the principle forces involved are both gravitational and viscous forces. For example, a sphere with diameter 10 μm dragged at 20 μm/s through water will feel a force of 2 pN. The force of gravity on this same sphere is 5 pN. To move the sphere horizontally at 20 μm/s requires laser power $\geq$ 1.3 mW,[14] while vertical translation requires laser power $\geq$ 12.5 mW.[14]

In the first half of this paper we will derive the trapping forces in the Mie regime, where the wavelength of light is much smaller than the diameter of the object. In this regime, we can neglect the wave properties of light and use the Ray-Optics model. We will also discuss a useful geometrical model that explains the less intuitive aspects of trapping. Next we will discuss the procedures of building a laser tweezer, followed by experimental results from calibrating the trapping forces. To simplify matters in both the theoretical and experimental sections, we deal only with uniform spheres.

III. Theory

At the most basic level, optical tweezers work by taking advantage of the momentum of light. Specifically, when a ray of light hits a sphere the momentum of that ray will change when reflected or refracted. As mentioned above, the change in momentum of the light causes an equal, but opposite, change in momentum of the sphere. The radiation force is just the change in momentum of the sphere per second. Trapping occurs when these forces are balanced over the sphere to give a net force of zero and a sufficiently deep potential well to hold the sphere against viscous, thermal and other perturbations. We will discuss the forces involved in a few simple cases.

To see how the optical force can lead to trapping, we will decompose the optical force into two components, the scattering component and the gradient component. A. Ashkin[14] defines the scattering force as the component of the radiation force in the direction of propagation of the laser. The gradient force is then the component of the force perpendicular to the laser's propagation direction.

For parallel rays of light hitting a sphere, Ashkin[14] gives the following expressions for the gradient and scattering forces of an individual ray:

$$F_{\text{scat}} = \frac{n_1 P}{c}\left\{1 + R\cos(2\theta) - \frac{T^2[\cos(2\theta - 2r) + R\cos(2\theta)]}{1 + R^2 + 2R\cos(2r)}\right\} \tag{1.1}$$

$$F_{\text{grad}} = \frac{n_1 P}{c}\left\{R\sin(2\theta) - \frac{T^2[\sin(2\theta - 2r) + R\sin(2\theta)]}{1 + R^2 + 2R\cos(2r)}\right\} \tag{1.2}$$

where P is the ray's power, θ is the angle the incoming ray makes with the normal to the surface of the sphere, and r is the angle the first transmitted ray makes with the perpendicular to the normal (see figure 1). R and T are the Fresnel coefficients of reflection and transmission, with R defined as the fraction of the light intensity reflected from the surface, and T being the fraction transmitted through the surface. The term $\left(\frac{n_1 P}{c}\right)$ represents momentum per second carried by light of power P.

The complexity of these expressions comes from summing over the all the rays—the reflected ray, the transmitted ray, and all of the internally reflected rays.[14] To simplify matters, we will ignore the higher order terms from the internal reflections and look only at the forces from the reflected ray and the first transmitted ray. Further, we consider two cases: a totally reflecting sphere (i.e., $R = 1$ and $T = 0$) and a totally transmitting sphere (i.e., $R = 0$ and $T = 1$). We will first look at the case of a totally reflecting ball.

A. Reflecting Sphere

For $R = 1$and $T = 0$, equations (1.1) and (1.2) become:

$$F_{scat}(R) = \frac{n_1 P}{c}\{\cos(2\theta) + 1\} \tag{1.3}$$

$$F_{grad}(R) = \frac{n_1 P}{c}\{\sin(2\theta)\} \tag{1.4}$$

We can see how equations (1.3) and (1.4) arise by considering the geometry and conservation of momentum.

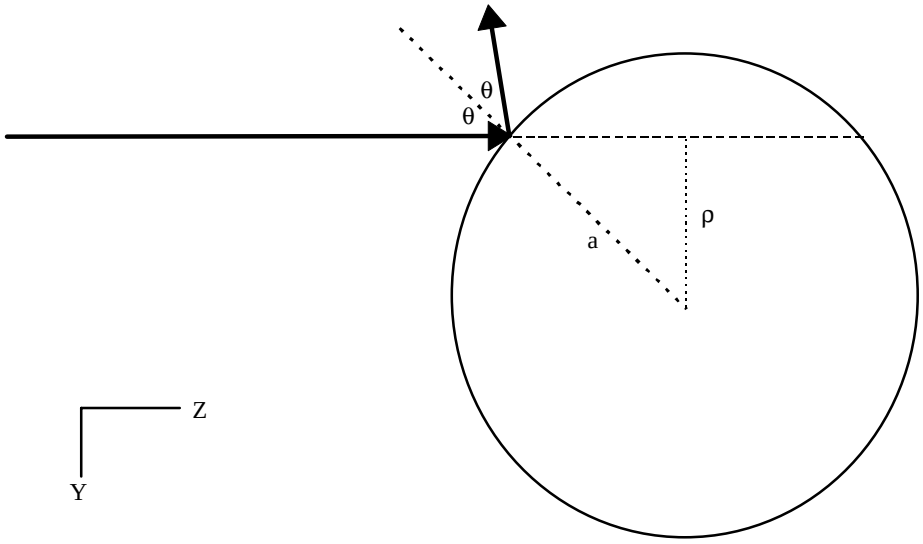

Figure 1 Geometry of a ray hitting a totally reflecting sphere. The solid lines demarcate the path of the ray and the dotted; dashed lines serve in the geometric proof. ρ is the perpendicular distance from the ray to the center of the sphere; *a* is the radius of the sphere.

In the *Z* direction, the momentum of the ray changes from $\left(\frac{n_1 P}{c}\right)$ to the resulting component in the *Z* direction, $\left(\frac{n_1 P}{c}\right)$ cos 2θ, giving us equation (1.3) for the scattering force. In the *Y* direction, the ray has no initial momentum so the momentum imparted to the ball has the same magnitude but opposite sign of the reflected ray in the *Y* direction, $\left(\frac{n_1 P}{c}\right)$sin 2θ.

B. Transmitting Sphere

For the totally transmitting case equations (1.1) and (1.2) become

$$F_{scat}(T) = \frac{n_1 P}{c}\{1 - \cos(2\theta - 2r)\} \qquad (1.5)$$

$$F_{scat}(T) = \frac{n_1 P}{c}\{\sin(2\theta - 2r)\} \qquad (1.6)$$

To see the origin of these forces, we use the same conservation of momentum arguments, but more complicated geometry, as shown in figure 2.

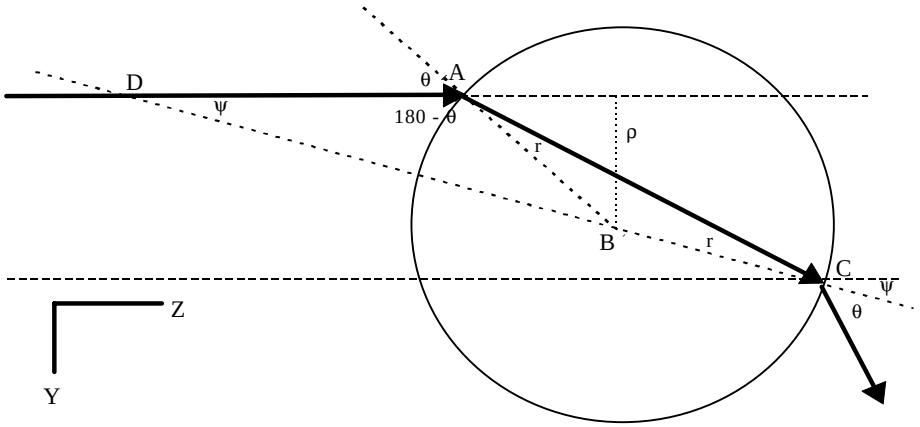

Figure 2 Geometry of a ray through a totally transmitting sphere.

The derivation of the $(2\theta - 2r)$ angular dependence proceeds in three steps. In terms of figure 2, the task is to show $\psi + \theta = 2\theta - 2r$.

1. Triangle *ABC* is isosceles, therefore $\angle ACB = \angle CAB = r$
2. Looking at triangle DAC, we see $\psi = 180 - (180 - \theta + r) - r = \theta - 2r$
3. Thus the change of the ray's angle with respect to *Z* is $\psi + \theta = 2\theta - 2r$

C. Conservative Forces

The next step is to write these expressions for reflecting and transmitting spheres in terms of the perpendicular distance from the ray to the sphere's center, ρ. Writing the forces in terms of ρ allows us to show that the gradient force is conservative[14] and to draw closer to showing how a trapping potential well arises. From the figures 1 and 2 we see that $\rho = -a \sin\theta$, taking θ to be positive in the clockwise direction and the direction of Y as defined in figures 1 and 2. We obtain the following expressions for the forces:

$$F_{scat}(R) = \frac{n_1 P}{c} \{1 - (\rho/a)^2\} \qquad (1.7)$$

$$F_{grad}(R) = \frac{n_1 P}{c} (\rho/a)\{1 - (\rho/a)^2\}^{1/2} \qquad (1.8)$$

$$F_{scat}(T) = \frac{n_1 P}{c} (\rho/a)^2 \{2 (n_1/n_2)^2 (\rho/a)^2 + 2 (n_1/n_2) [1 - (\rho/a)^2]^2 [1 - (n_1/n_2)^2 \quad (\rho/a)^2]^2 - (n_1/n_2)^2 - 1\} \qquad (1.9)$$

$$F_{grad}(T) = \frac{n_1 P}{c} (\rho/a) \{ [1 - (\rho/a)^2]^{1/2} [1 - 2 (n_1/n_2)^2 (\rho/a)^2 - (n_1/n_2) [1 - (n_1/n_2)^2 (\rho/a)^2]^{1/2} \quad (1 - 2 (\rho/a)^2) \} \qquad (1.10)$$

Plotting these expressions in terms of ρ, we get:

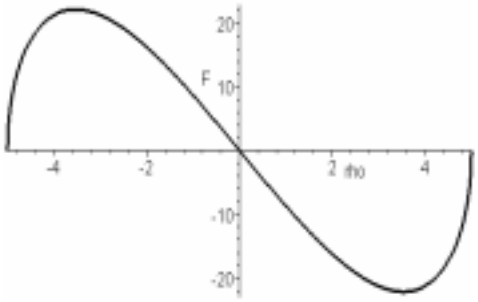

Figure 3 Reflecting gradient force, with incident power P = 5 mW. Distance is in μm and force is in pN.

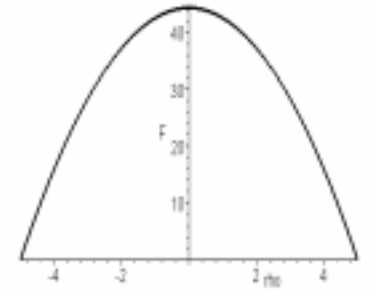

Figure 4 Reflecting scattering force, with incident power *P* = 5 mW. Distance is in μm and force in pN.

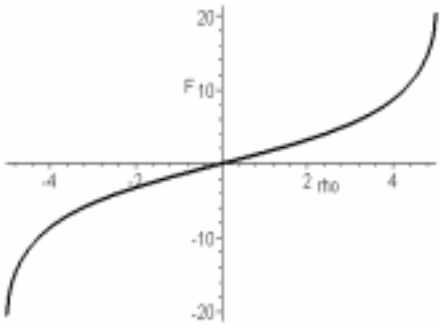

Figure 5 Transmitting scattering force, with incident power *P* = 5 mW. Distance is in μm and force is in pN.

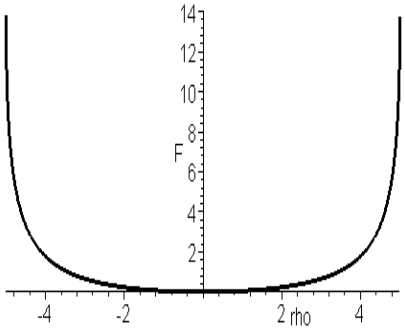

Figure 6 Transmitting gradient force, with incident power *P* = 5 mW. Distance is in μm and force is in pN.

These plots show that only the transmitting gradient force will lead to trapping with parallel rays. For positive ρ, the transmitting gradient force yields a positive force which draws the center of the sphere toward the beam until the beam passes through the center of the sphere, at which point the force is zero.

In our simplified model up to this point, we have assumed that all of the power of the laser, *P*, is delivered to the sphere by a single ray. In actuality, however, the laser hits the sphere as a laser intensity distributed over a surface. Therefore, we treat the forces mentioned thus far as differential elements of force

and the differential power, *P*, as an intensity, denoted by *I*. Now, the total force on the sphere is the differential elements of force integrated over the surface of the sphere. This integration is a simple matter for scattering forces because they point in the direction of the incident ray. For the scattering cases we integrate over the surface of the hemisphere closest to the beam, with $\theta = 0$ along the beam axis. Thus we integrate from $\theta = 0 \ldots \pi/2$, and $\phi = 0 \ldots 2\pi$. We use the substitution $\rho = -a \sin\theta$ as seen from figures 1 and 2 to obtain:

$$F_{scat}(R,Tot) = \frac{n_1 I}{c} \iint \{1-(\rho/a)^2\}\, a^2 \sin\theta \, d\theta \, d\phi$$

$$= \frac{n_1 I}{c} \iint \{1-(-a \sin\theta/a)^2\}\, a^2 \sin\theta \, d\theta \, d\phi$$

$$= \frac{2\, n_1 I \pi a^2}{3\, c} = \frac{n_1 I V_{sphere}}{2\, a\, c} \qquad (1.11)$$

$$F_{scat}(T, Tot) = \frac{n_1 I}{c} \iint \{(\rho/a)^2 \{2 (n_1/n_2)^2 (\rho/a)^2 + 2 (n_1/n_2) [1 - (\rho/a)^2]^{1/2} [1 - (n_1/n_2)^2 \quad (\rho/a)^2]^{1/2} - (n_1/n_2)^2 - 1\} \}\, a^2 \sin\theta \, d\theta \, d\phi$$

$$= \frac{n_1 I}{c} \iint \{(-a \sin\theta/a)^2 \{2 (n_1/n_2)^2 (-a \sin\theta/a)^2 + 2 (n_1/n_2) [1 - (-a \sin\theta/a)^2]^{1/2} [1 - (n_1/n_2)^2 \quad (-a \sin\theta/a)^2]^{1/2} - (n_1/n_2)^2 - 1\} \}\, a^2 \sin\theta \, d\theta \, d\phi$$

$$= \frac{4\, n_1 I \pi a^2}{15\, c\, (n_1/n_2)^3} \{ [2 + (n_1/n_2)^2 - 3 (n_1/n_2)^4] \sqrt{1-\left(\frac{n_1}{n_2}\right)^2} - 2 + 5 (n_1/n_2)^3 - 3 (n_1/n_2)^5\}$$

$$= \frac{n_1 I V_{sphere}}{5\, a\, c\, (n_1/n_2)^2} \{ [2 + (n_1/n_2)^2 - 3 (n_1/n_2)^4] \sqrt{1-\left(\frac{n_1}{n_2}\right)^2} - 2 + 5 (n_1/n_2)^3 - 3 (n_1/n_2)^5\} \qquad (1.12)$$

We have pulled the intensity out of the integral in equations (1.11) and (1.12) because we assume a constant intensity over the hemisphere. For a 5 mW beam

with a waist of 5 μm (and thus intensity I = 63.7 MW/m^2) hitting a polystyrene sphere (radius a = 5 μm and index of refraction n_2 = 1.6) in water (index of refraction n_1 = 1.33) we have $F_{scat}(R, Tot)$ = 14.8 pN and $F_{scat}(T, Tot)$ = 3.9 pN. As shown in figures 4 and 6, these forces from parallel rays will always push the ball in the direction of the beam's propagation, and will therefore not lead to trapping by themselves.

Unlike the scattering forces, the gradient forces do not point in the same direction, so we cannot integrate in the same manner. To sidestep this difficulty, we first convert the force into a scalar potential. Then we integrate this potential over the surface of the sphere.

$$U_{grad}(R) = -\int F_{grad}(R)\, d\rho = \frac{n_1 I \pi a^3}{3c} = \frac{n_1 I V_{sphere}}{4c}$$

$$= Q_{R=1} V_{sphere} \left(\frac{I}{c}\right) \qquad (1.13)$$

$$U_{grad}(T) = -\int F_{grad}(T)\, d\rho = \frac{-n_1 I \pi a^3}{60c} \{15 [(n_1/n_2)^2 - 1]^2 \ln [(1 + (n_1/n_2))/$$

$$(1 - (n_1/n_2))\,] - 24 (n_1/n_2)^6 + 20 (n_1/n_2)^4 - 30 (n_1/n_2)^3 + 34 (n_1/n_2)\,\}$$

$$= \frac{-n_1 I V_{sphere}}{80c} \{15 [(n_1/n_2)^2 - 1]^2 \ln [(1 + (n_1/n_2))/(1 - (n_1/n_2))\,]$$

$$- 24 (n_1/n_2)^6 + 20 (n_1/n_2)^4 - 30 (n_1/n_2)^3 + 34 (n_1/n_2)\,\}$$

$$= Q_{T=1} V_{sphere} \left(\frac{I}{c}\right) \qquad (1.14)$$

where we have introduce Q as a quality factor dependent upon n_1 and, in the transmitting case, n_2. For polystyrene (n_2 = 1.6) in water (n_1 = 1.33), we have $Q_{R=1}$ = 0.33 and $Q_{T=1}$ = 0.20. We notice in equations (1.11), (1.12), (1.13), and (1.14) that the term I / c is the energy density inside the sphere. Thus, when we multiply the volume of the sphere by I / c, we obtain the remarkable result that the

potential well and the restoring force are both proportional to the energy stored in sphere.

Since both expressions for the potential lack a dependence on the distance from the center of the sphere perpendicular to the axis of the beam, ρ, differentiating with respect to ρ gives a force of zero. This result is no surprise due to the symmetry of the problem. Nevertheless, if the intensity depends on position (as in a gaussian beam, for example) the potential will also depend on position, thereby producing a force. Assuming that the change in the intensity is small over the surface of the sphere, we can write the reflecting and transmitting gradient potentials by replacing the constant intensity I with $I(\rho)$.

We obtain the gradient force by taking the gradient of the above potentials. This operation yields a constant related to the physical characteristics of the sphere times the gradient of the intensity, hence the name "gradient force." We are now ready to write the general expression for the gradient forces for the scattering and reflecting cases.

$$F_{\text{grad}}(R) = \frac{-n_1 Q_{R=1} V}{c} \nabla I(\rho) \qquad (1.15)$$

$$F_{\text{grad}}(T) = \frac{-n_1 Q_{T=0} V}{c} \nabla I(\rho) \qquad (1.16)$$

For the specific case of a gaussian beam intensity $I(\rho) = I_o \exp(-\rho^2/w^2)$, with a 5 mW laser and a beam waist of $w = 5$ μm we have $I_o = 63.7$ MW / m^2. When this beam hits a ball of diameter 10 μm, equations 1.13 and 1.14 give us the following potentials:

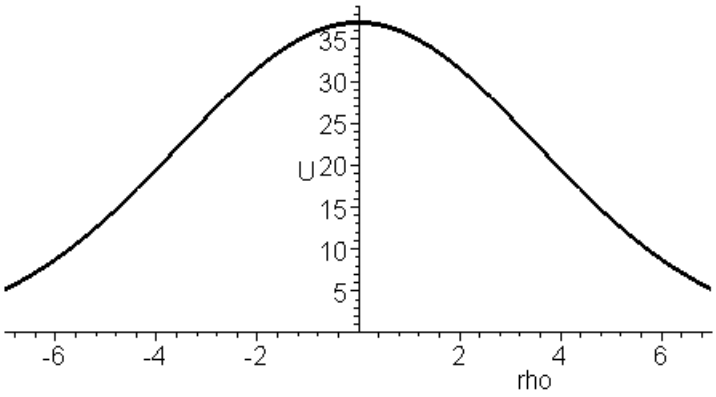

Figure 7 Gradient potential due to a gaussian beam on a reflecting sphere; ρ is in μm and potential is in 10^{-18} J = 1 pW μm.

From figure 7, we see explicitly that the reflecting gradient force will not trap a spherical ball.

The transmitting gradient potential, however, displays different behavior. This potential has the form:

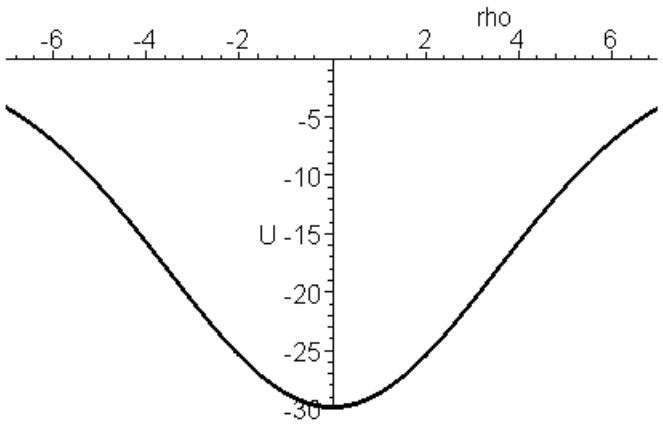

Figure 8 Gradient potential due to a gaussian beam on a transmitting sphere; position is in μm and ρ is in 10^{-18} J = 1 pW μm.

As a gauge on the magnitude of this potential well, we note that the thermal energy of a particle at room temperature is 0.00414 10^{-18} J. The transmitting gradient potential seems sufficiently deep to hold a particle against

thermal perturbations. To check against gravitational and viscous forces, we first compute the magnitude of the maximum restoring force for this well.

From figure 8 we see that the maximum restoring force occurs around $\rho = 3.5\ \mu m$, where the slope of the potential is greatest. We have $F_{grad}(T) = 5.1$ pN—enough to match gravity, as shown on page 4. The restoring force in the transmitting gradient case is also sufficient to drag a ball through water at speeds up to 54.1 μm / s. The situation described with the transmitting gradient force (i.e., trapping forces orthogonal to a parallel beam hitting a sphere) mirrors early trapping experiments by Ashkin[2] and Roosen.[8]

C. Geometrical Model

Using the principle that light must travel the same route forwards and backwards in time, we consider the reverse of previous case of parallel rays hitting a transmitting spherical ball. In our original case, the incoming rays have all of their momentum in the +*Z* direction. With the outgoing rays, however, only part of the momentum is in the +*Z* direction; the sphere refracts a portion of the momentum into +*Y* and -*Y*. Therefore, the change momentum of the light points in the -*Z* direction, giving the ball momentum in the +*Z* direction (see figure 9).

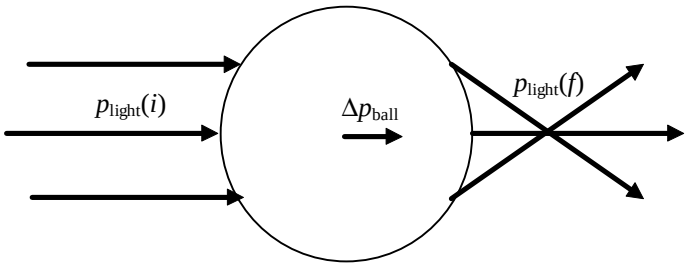

Figure 9 Momentum for parallel rays hitting a sphere

If we reverse the direction of the rays, with focused rays coming in from the right, and parallel rays emerging, we get a most counterintuitive result.

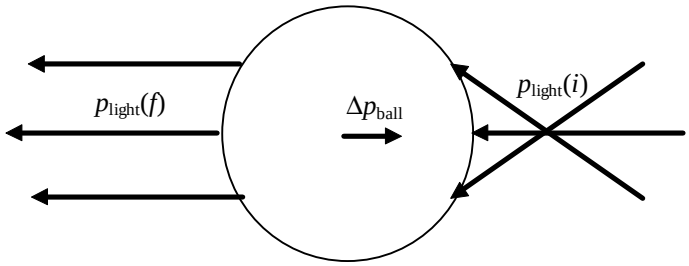

Figure 10 Momentum for focused rays hitting a sphere

Although everything else is reversed, the change in the momentum of the ball stays the same (see figure 10). Therefore, we see how a laser tweezer can pull an object toward the direction of propagation of the light. We also conclude that the maximum restoring force for a transmitting sphere is exactly equal to the scattering transmitting force with parallel rays (see equation (1.12)).

This model also enables a first-pass calculation of the maximum restoring forces in transverse directions. Our calculation proceeds by considering the energy required to remove a sphere from the trap. While the climb out of the well is steeper in some directions than others, the depth of the well is constant and the work required to remove a sphere from the well is the same regardless of the direction of removal.

We assume that the maximum restoring force will occur half way up the potential well where the derivative of the potential is greatest, as was the case in figure 8. In the *Z* direction, the work to move the ball Δz is

$$U_z = F_z\,(avg)\,\Delta z \qquad (1.17)$$

We approximate $F_z\,(avg)$ by summing the maximum and minimum forces on Δz and dividing by two. From our geometrical model, we know that $F_z\,(min)$ is zero

and occurs when the focus of the laser coincides with the center of the ball (assuming total transmittance). We also know F_z (*max*) is equal and opposite to the scattering transmitting force from parallel rays ($F_{scat}(T)$ from equation (1.12)). Δz is the distance between the positions of the minimum and maximum forces. For our model, $\Delta z \approx a$, the radius of the sphere. We now have

$$U_z = \frac{F_z\,(max) + F_z\,(min)}{2}\,\Delta z = \frac{F_{scat}\,(trans,\, total)}{2}\,a \qquad (1.18)$$

This value for potential energy will also equal the work required to remove the ball in the *Y* or *X* direction. Again, we know the minimum force occurs at the bottom of the well and equals zero. From the work relation, we can approximate F_y (*max*) and F_x (*max*) (the two are identical in our model). In the transverse direction, however, we are moving the ball completely out of the well, not just from the force minimum to maximum. We know, however, that this distance equals *a*, because once the ball has been moved one radius from the trap center (assuming a small spot size), the ball is free of the trap. We then approximate that F_y (*max*) occurs at a distance ½ *a* from the trap center. We now have

$$U_y = \frac{F_y\,(max) + F_y\,(min)}{2}\,\Delta y = \frac{F_y\,(max)}{2}\,\frac{a}{2} = U_z \qquad (1.19)$$

and therefore

$$F_y\,(max) = \frac{4\,U_z}{a} = 2\,F_{scat}\,(T,\, Tot) = (2)\,(3.9\text{ pN}) = 7.8\text{ pN}$$

where we assume the laser has intensity $I = 63.7$ MW / m^2 and use $n_1 = 1.33$ and $n_2 = 1.6$ in equation (1.12) for a sphere of radius 5 μm. Appealing to the Stokes drag law, we should be able to pull such a sphere through water at 82.8 μm/s with this force.

III. Experimental Methods

As we see from the geometrical model, the main goal in building the laser tweezer is to maximize the power focused tightly on the ball.

A. Choosing components

To obtain trapping we need sufficient power to overcome viscous, gravitational, and thermal forces. The viscous force takes the form of the Stokes drag force for spheres:

$$F_d = 6 \pi \eta a v_c \tag{1.20}$$

where η is the viscosity of water, a is the radius of the ball, and v_c is the velocity of the ball. For a ball having radius 5 μm ball moving at 20 μm per second, and taking $\eta = 10^{-3}$ N s / m^2, the drag force is 2 pN. Trapping forces can be expressed in the form

$$F = Q \frac{n_1 P}{c} \tag{1.21}$$

where Q is the quality factor discussed in the theory section. A typical value that accounts for both reflection and transmission is $Q = 0.25$.[14] Thus, to drag a ball with a diameter of 10 μm at 20 μm / s we would need 1.5 mW of power. In order to allow for loss factors and ensure trapping, we chose a 28 mW laser with a wavelength of 675 nm and FWHM beam size at the output of 1.9 mm x 0.6 mm. We chose a wavelength in the red to ensure the visibility of the beam and to minimize thermal damage to samples. Moreover, a 675 nm laser makes it possible to explore the theoretically perplexing situation in which the laser wavelength and the object are of the same size.

The second chief component of the trap is the microscope objective lens. We can get an idea of the lens parameters required from our geometrical model.

Parallel rays hitting a sphere 10 μm in diameter will focus the beam 4.65 μm from the far side of the sphere (see figure 11). We need an objective lens that will mirror the focusing behavior of the sphere. A useful quantity here is the F/number, defined as the focal length of a lens over its diameter. Our objective lens should have an F/number close to that of our sphere, so that triangles *ABC* and *DEC* will remain similar for large values of α. We are concerned with large values of α because those rays experience the greatest change in momentum the *Z* direction when focused through the sphere.

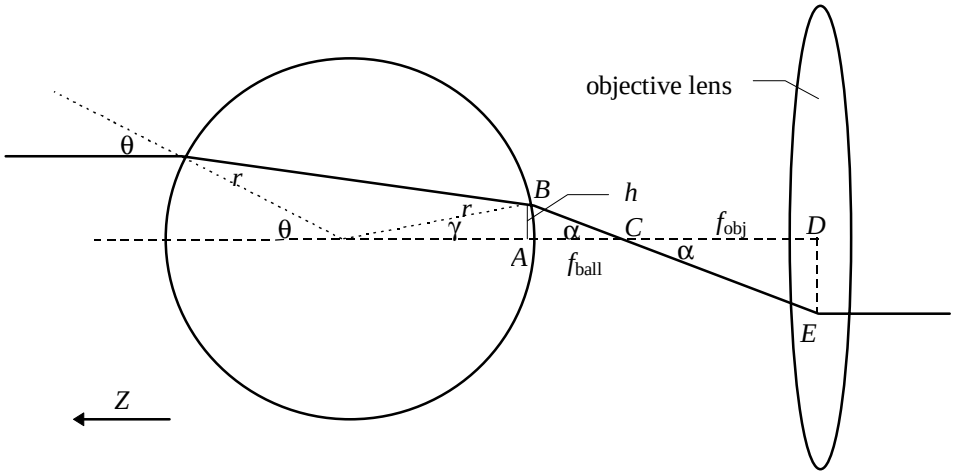

Figure 11 Geometry for determining the F/number. From figure 2, we know a = 2θ - 2*r*. We notice γ = 2*r* - θ, making *h* = sin γ. Finally, $f_{ball} = h / \tan \alpha$. Notice triangles *ABC* and *DEC* are similar.

From these considerations, we see that our objective lens should have an F/number = 0.465. In microscopy, however, objective lenses are characterized by the numerical aperture, NA, where NA = *n* sin α, with *n* being the index of refraction of the medium, and α being the half-angle of the focused cone of light, as in figure 11. Our calculated F/number corresponds to NA ≈ 1.1. We use a Leitz Wetzlar oil immersion objective with NA = 1.3. In terms of intensity gradients (as in equations (1.15) and (1.16)), using a high NA lens maximizes the intensity gradient and thus the gradient forces.

The final component question is what size balls to use. Duke Scientific offers silica microspheres ranging from 0.5 μm to 1.6μm in diameter. Bangs Laboratories carries polystyrene balls with diameters from 0.5 μm to 25 μm. We chose 10 μm polystyrene balls for ease of viewing and trapping.

B. Optics Setup

The job of the optics is to deliver the light from the laser module to the back of the objective lens so that the beam fills the objective lens and hits the objective at the appropriate angle to minimize the spot size. Please refer to figure 12 for our optics layout. If the beam waist at the objective, d_{obj}, is less than the diameter of the objective lens, D_{obj}, the angle subtended by the focused light cone will be smaller that if $d_{obj} = D_{obj}$, thereby decreasing the NA, and increasing the spot size according to eq (1.22). If $d_{obj} > D_{obj}$, the NA will be optimized, but the light outside of D_{obj} can contribute nothing to the trap, and is lost.

The first step, however, is to align the mirrors to deliver the light to the objective lens (see fig. 12). Mirrors M_1 and M_2 are useful as beam steerers, while M_5 is a dichroic mirror which reflects red light at 45°, but transmits all other light. With the mirrors in place, we choose appropriate lenses (detailed below) and realign the system. If the beam is hitting the lenses in the center and if the lenses meet the beam at right angles, the beam will not be diverted.

Our laser's smaller FWHM waist is 0.9mm, so to fill our objective lens ($D_{obj} \approx 2$ mm), we must double the beam waist. We expand the beam using lenses L_1 and L_2, where $f_1 = 50.8$ mm and $f_2 = 101.6$ mm . The lenses are spaced a distance $d = f_1 + f_2$ apart, so we have magnification $M = -f_2 / f_1 = -2$, which gives us a collimated beam after L_2 with diameter D_{obj}.

The next step is to focus the beam to fill the objective lens and hit the lens at an angle that minimizes spherical aberrations. When filling a lens with light, the thin lens approximation breaks down for the rays near the perimeter of the lens. The focal length near the perimeter is less than in the center, so the rays near the perimeter focus to a different point than the rays near the center. This effect, called

spherical abberation, increases the spot size, and thus decreases the amount of power delivered to the microsphere. To counter this effect, we send in diverging, rather than parallel rays. Specifically, we use lens L_3 to focus our collimated beam to a spot 17 cm from the objective, so that the light hitting the objective subtends the best angle to minimize spherical aberrations. For our microscope, this means L_3 must have a focal length f_3 = 85 mm.

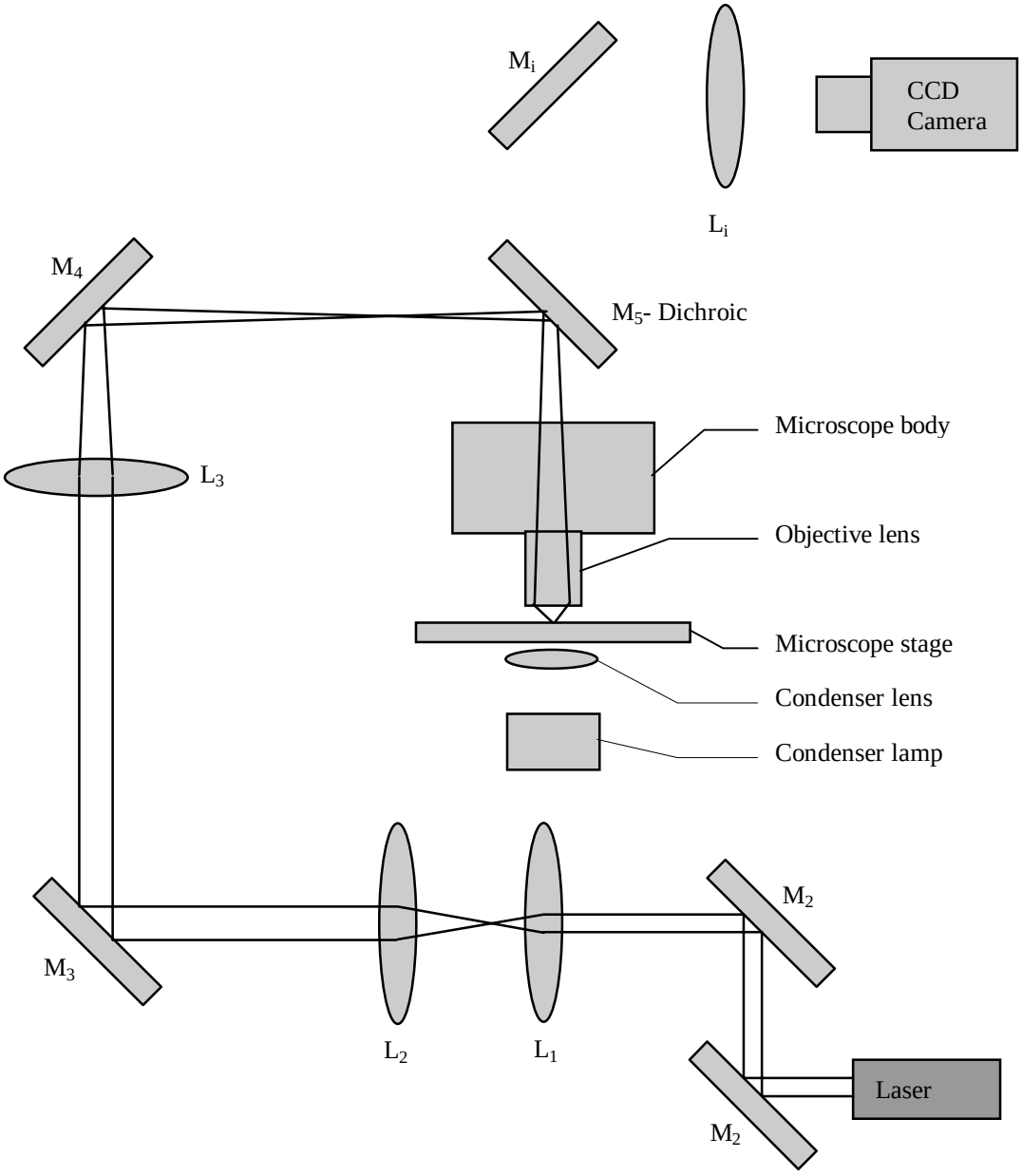

Figure 12 Laser tweezer set-up

If we treat the focal point of L_3 as an object to be imaged through the objective, we can calculate the location of the trap using the Lens Equation. With $d_o = f_3 = 85$ mm and $f_{obj} = 2.0$ mm, $d_i = 2.05$ mm gives the position of the trap focus.

Once the basic optics are set up (see figure 12), we make sure everything is aligned correctly. To check that the lenses are perpendicular to the beam, we pass the beam through a pinhole before the lens and align the reflected light from the lens surface back through the pinhole opening.

C. Imaging System

We use a Schumberger CCD camera connected with BNC cables to a monitor-VCR system to observe and record trapping. But first, we need the imaging system to be focused in the same plane as the laser. The simplest way to match these focal planes is to think of the imaging system as the trap in reverse. Thus the object is now the trap itself, which is imaged a distance 85 mm from the objective lens (see fig. 13). To look at the microspheres in the plane of the trap, we need to image onto the spot 85 mm from the objective lens. With a 195.6 mm focal length lens, we position the lens approximately 517 mm from the objective lens; we place the CCD camera about 936 mm behind the imaging lens, as dictated by the ray-tracing diagram in figure 13.

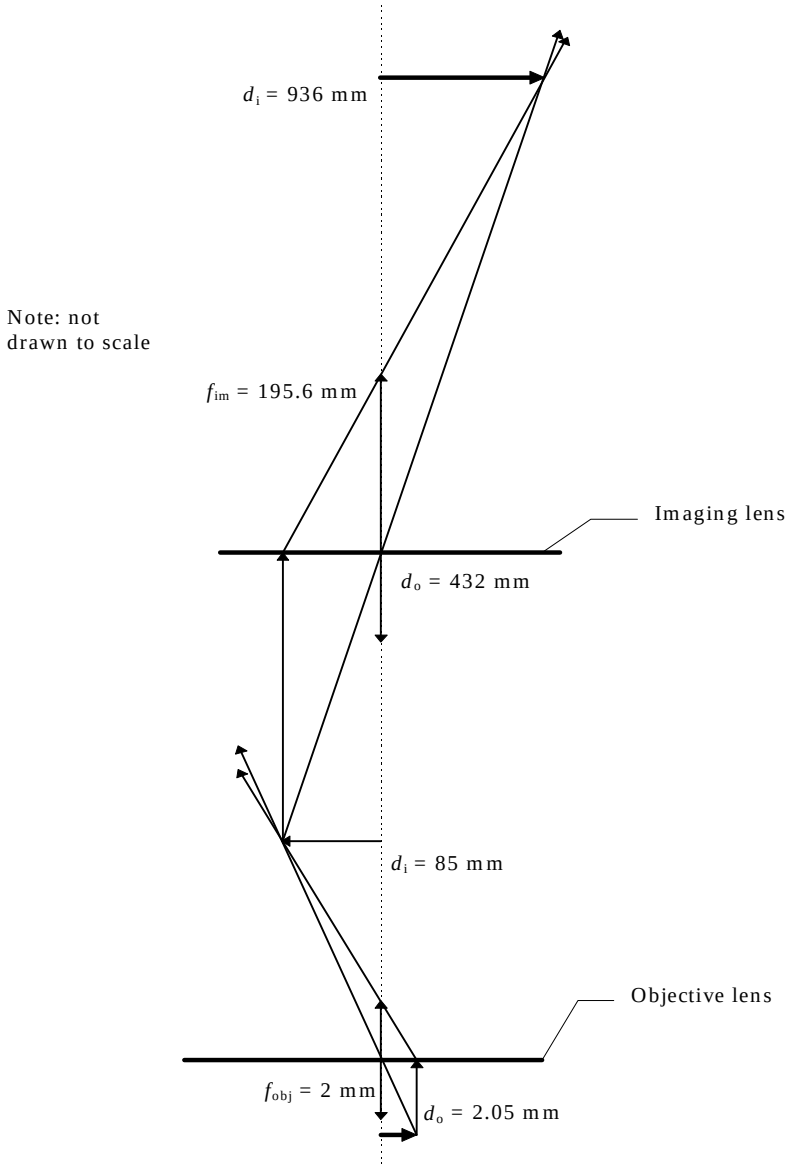

Figure 13 Ray-tracing diagram of imaging system

IV. Results

We now turn to testing our trap, and characterizing the potential well.

A. Evidence of Trapping

The first step in checking for trapping is to locate the laser in the field of view. With a dichroic mirror matched exactly to the wavelength and angle of incidence, we would not see the laser through the CCD camera. Our dichroic

mirror, however, does not match the wavelength and angle of incidence perfectly, so we can see the laser's reflection in our camera. Once we find where the laser's focus reflects off the top cover slip, we have a good sense of where the trap will be. After moving the laser further into the sample, we start to look for trapping.

The best manner of determining if a ball is trapped is to move the translational stage of the microscope slowly. If the trapping candidate stays still but the other balls move with the stage, then the ball has been trapped in two dimensions. To test for three dimensional trapping, we move the stage up and down. If a ball is trapped vertically, it will stay in focus while the other balls move into and out of focus.

We have achieved consistent trapping in the two dimensions orthogonal to the laser beam (see figure 14).

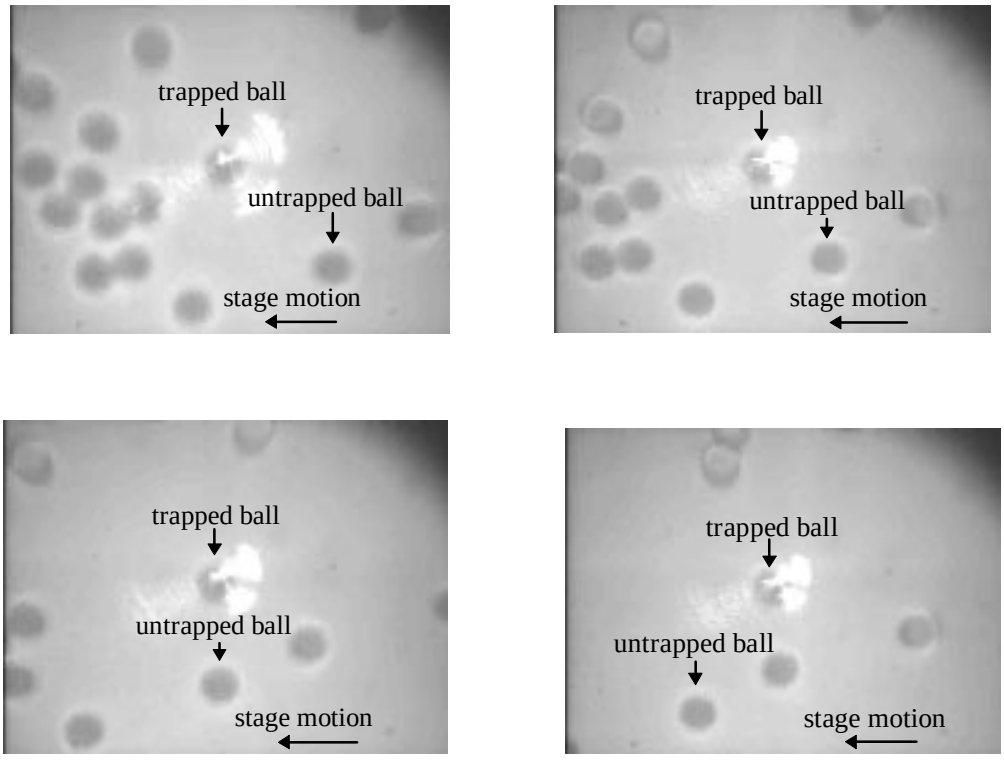

Figure 14 Demonstration of trapping perpendicular to the beam

B. Measurement of the Trapping Forces

We measure the maximum transverse trapping force by trapping a sphere and then translating the stage at an increasing velocity until the ball breaks free of the trap. The velocity just before the ball breaks from the trap is the escape velocity, which we can use in the Stokes drag force (equation 1.19). We record the escapes on a VHS tape in SP record mode, giving us a capture rate of 30 frames per second. Using Intel Smart Video Recorder Pro software, we transfer the footage to an ".avi" file. We then use an Excel program written by W.E. Cooke to track the velocity of the trapped ball. To calculate the velocity, we plot the position of the ball as a function of time and fit the plot to a quadratic.

We obtain the error plots by subtracting the measured position from the calculated position given by the fit. When the error plot shows a significant trend near the point of escape, we calculate another fit, using only those points included in the trend.

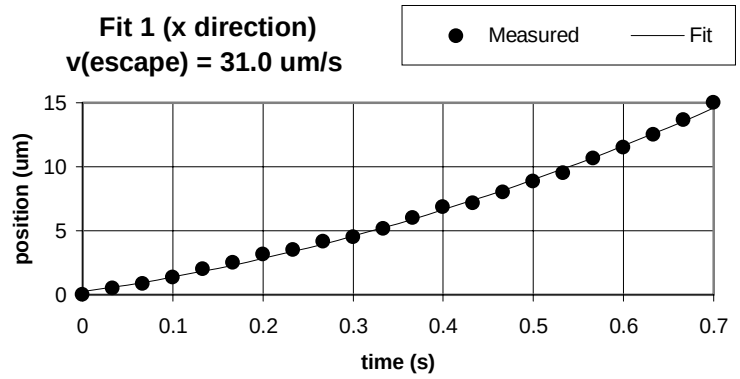

Figure 15 Position measurements and fit from data set 1; position is in the *X* direction

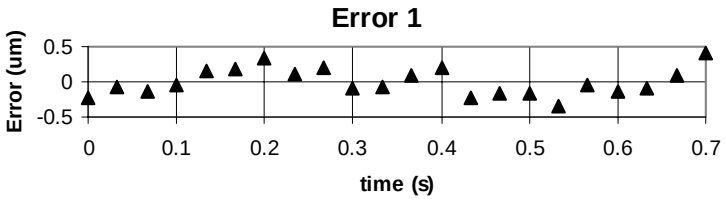

Figure 16 Error in set 1

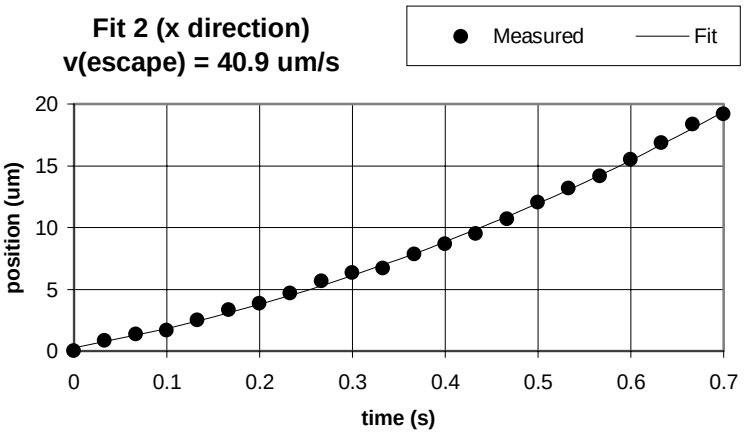

Figure 17 Position measurements and fit for data set 2; position is in the *X* direction

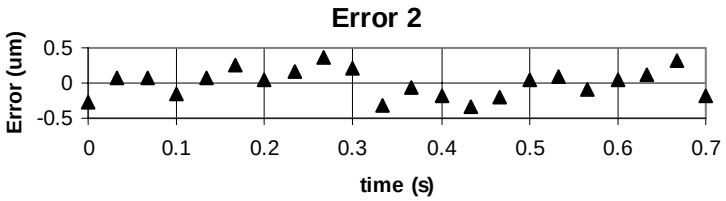

Figure 18 Error in set 2

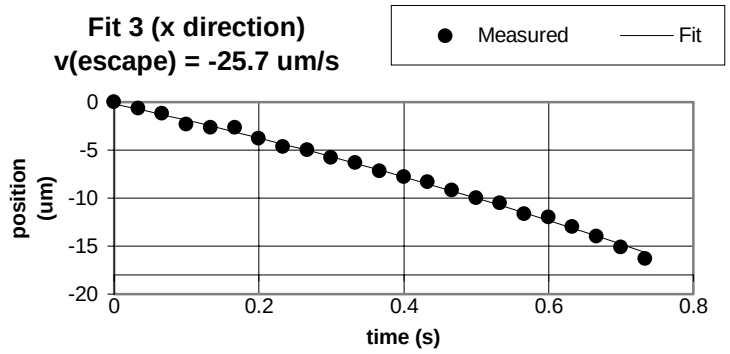

Figure 19 Position measurements and fit for data set 3; position is in *X* direction

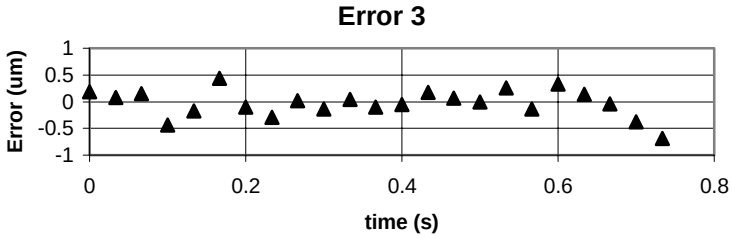

Figure 20 Error in set 3

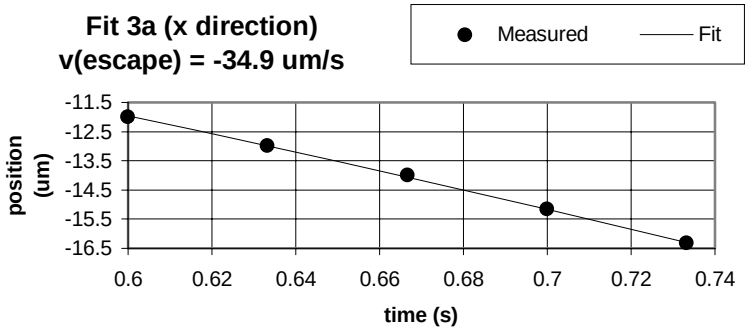

Figure 21 Position and fit for data set 3a, consisting of the last 6 points of set 3

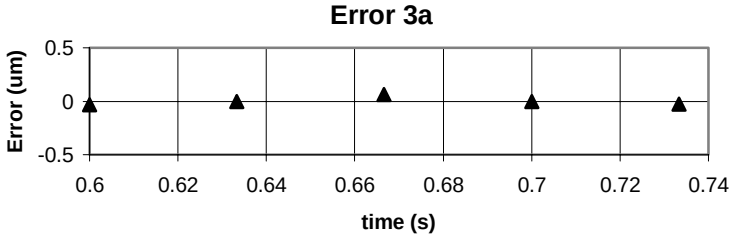

Figure 22 Error in set 3a

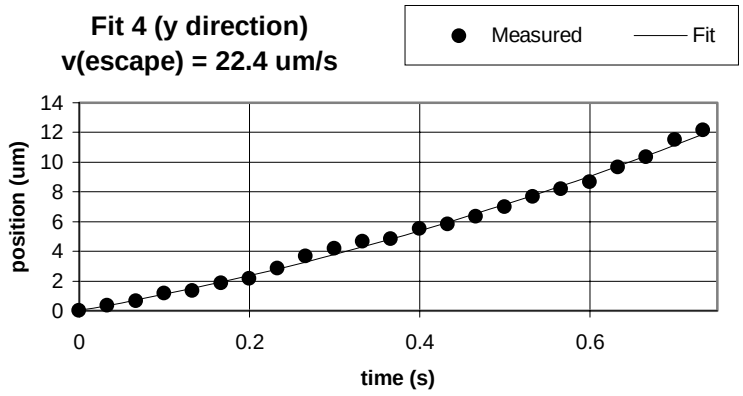

Figure 23 Position measurements and fit for data set 4; position is in Y direction

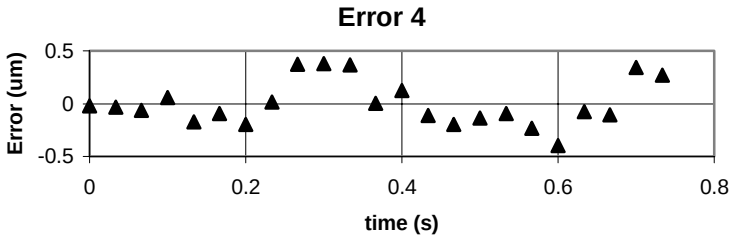

Figure 24 Error in set 4

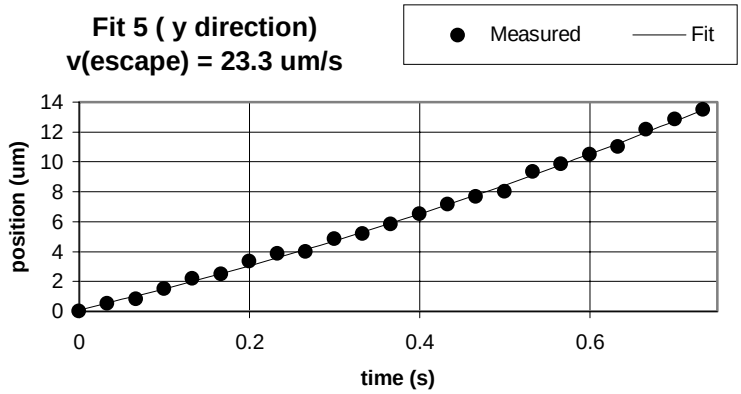

Figure 25 Position measurements and fit for data set 5; position is in the Y direction

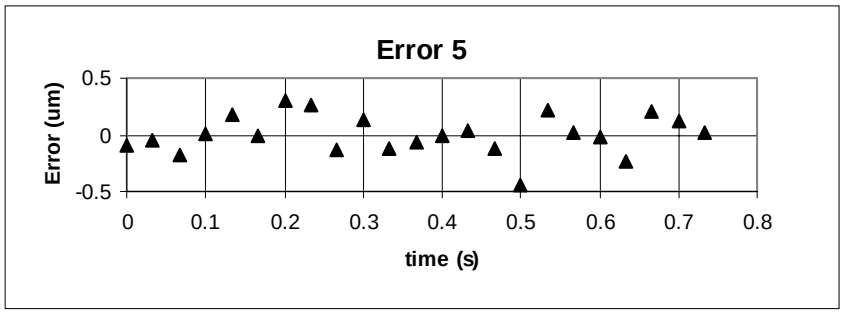

Figure 26 Error in set 5

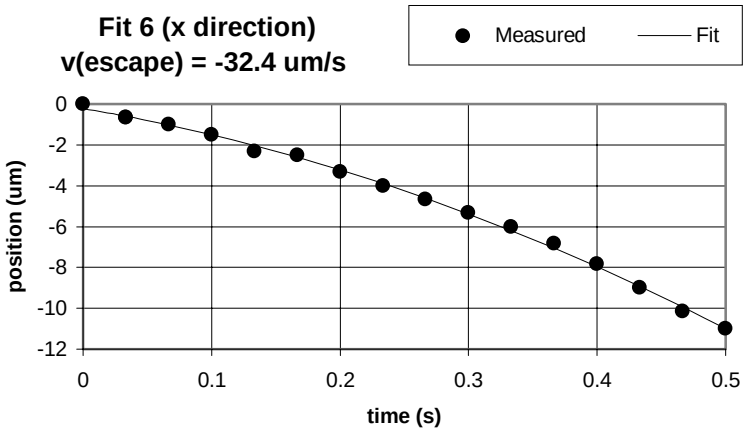

Figure 27 Position measurements and fit for data set 6; position is in the *X* direction

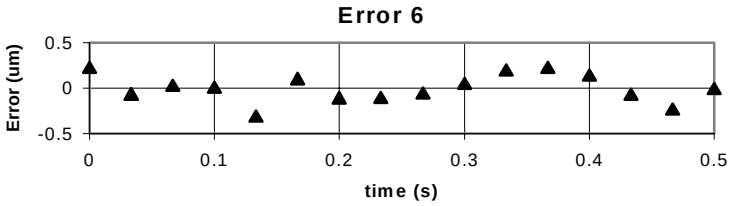

Figure 28 Error in set 6

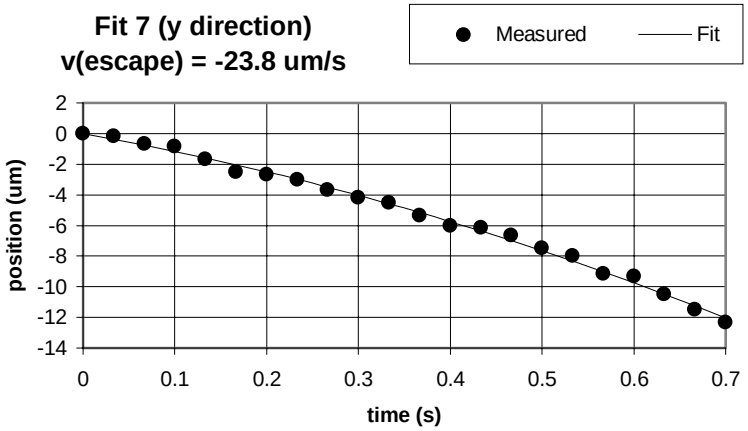

Figure 29 Position measurements and fit for data set 7; position is in the *Y* direction

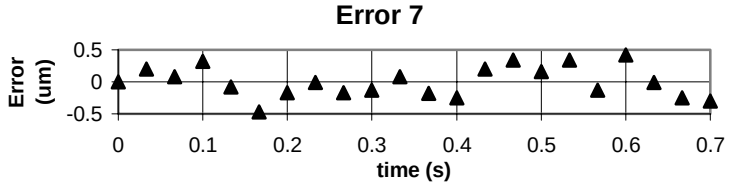

Figure 30 Error in set 7

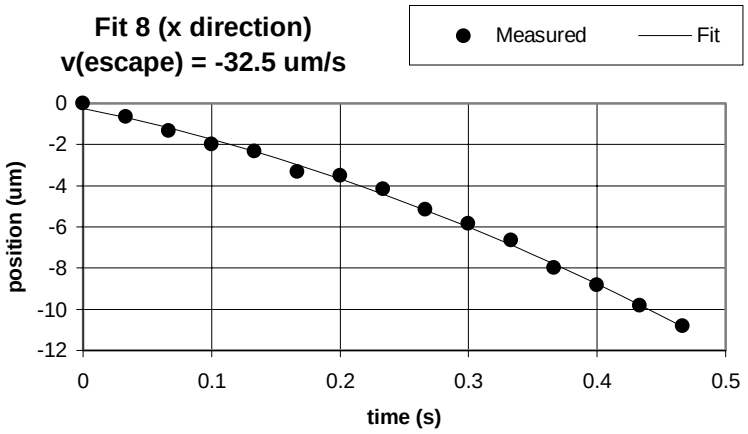

Figure 31 Position measurements and fit for data set 8; position is in the *X* direction

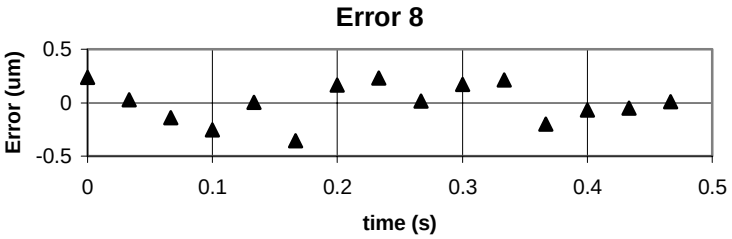

Figure 32 Error in set 8

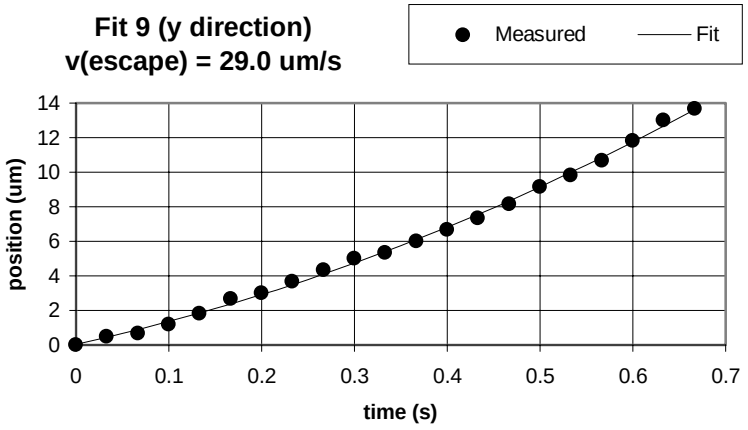

Figure 33 Position measurements and fit for data set 9; position in the Y direction

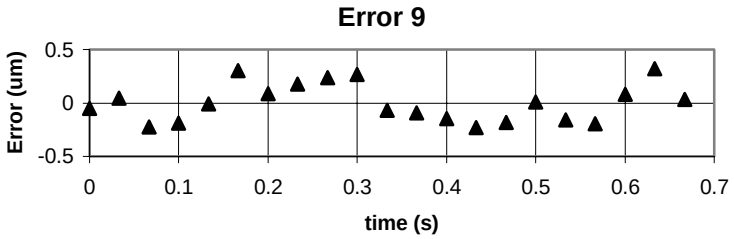

Figure 34 Error in set 9

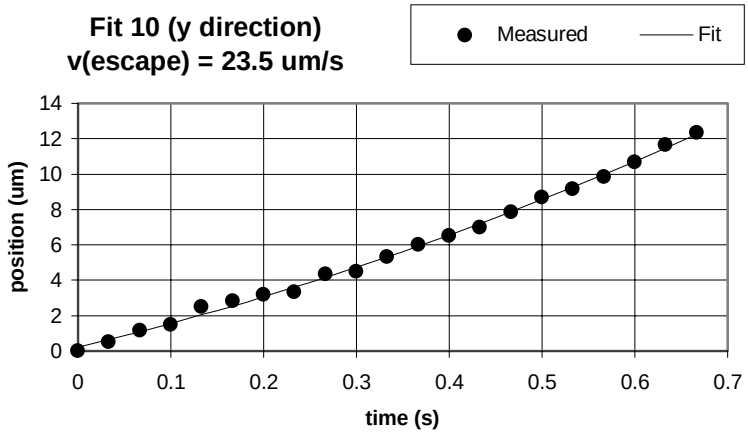

Figure 35 Position measurements and fit for data set 10; position is in the *Y* direction

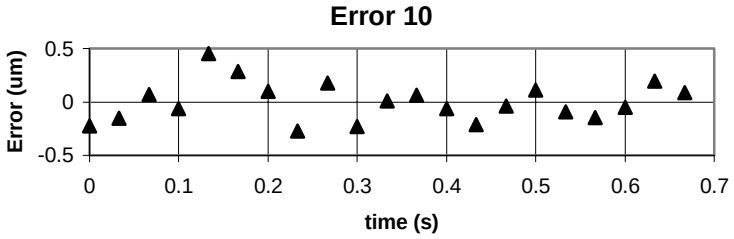

Figure 36 Error in set 10

From these plots, we have the following measurements for escape velocities and maximum trapping forces in the *X* and *Y* directions:

Data Set	v (um/s)	Fd (pN)
1	37.9	3.571991
2	40.9	3.854734
3	-34.9	-3.28925
6	-32.4	-3.05363
8	-32.5	-3.06305

Figure 37 Escape velocity and maximum trapping force in *X* direction

Data Set	v (um/s)	Fd (pN)
4	22.4	2.11115
5	23.2	2.186548
10	23.5	2.214823
9	29.0	2.733186
7	-23.8	-2.2431

Figure 38 Escape velocity and maximum trapping force in *Y* direction

That the trap is almost twice as strong in the *X* direction as in the *Y* direction is probably due to the asymmetry of the beam entering the objective lens. The beam is highly oblate (recall fwhm diameter = 1.9 mm x 0.6 mm), so in adjusting the beam diameter at the objective we straddle the two related problems. Either we underfill the objective along the short axis, thus decreasing the focusing angle, α (see figure 11) or we overfill along the long axis, thus wasting power in that direction. A fix to this problem would be to insert a cylindrical lens to give a more circular beam profile.

V. Future Work

A few improvements to the current set-up hold promise to improve trap performance and data. Besides the cylindrical lens mentioned above, we could reduce loss by eliminating mirrors M_1, M_2, M_3, and one additional mirror before lens L_3 not shown in figure 12. We could also replace the first surface mirrors used (which reflect about 70% of incident light) with dielectric mirrors (which reflect about 99% of incident light). To illustrate the extent of the power loss through our set-up, we drop from 27 mW at the laser to 7.4 mW before the objective lens.

Another problem was the non-constant acceleration of the microscope stage during escape velocity measurements, as evidenced by figures 15 through 36.

A motorized stage would provide constant acceleration, thus improving the quadratic fits to the position as a function of time.

Although we have consistently demonstrated two-dimensional trapping, three-dimensional trapping should be possible with our set-up. We once witnessed three dimensional trapping, but we were unable to reproduce the event on film.

VI. Conclusion

We have analyzed simplified models of laser trapping in the Mie regime and proposed a geometrical model for calculating the maximum trapping force. While our model yields forces larger than what we observed, it proved useful in understanding three-dimensional trapping and in determining what optics to use.

Moreover, when we take into account that a significant fraction of laser power was lost due to the oblate shape of the beam, our result becomes more realistic. Our observations indicate that shape causes about one half of the laser power just before the objective to be lost. Our maximum force in the X and Y directions then becomes 5.8 pN, rather than the 7.8 pN we had calculated for an incident beam of 5 mW (we also use our measured laser power before the objective of P = 7.4 mW).

The remaining difference from the measured trapping forces most likely arises from the idealizations used in the model. We assumed the thin lens approximation in saying that the parallel incident light would focus to a point (see figure 9). For rays away from the center of the sphere, though, spherical aberrations factor in, giving different focal lengths for different values of the perpendicular distance from the ray to the center of the sphere. In reverse (see figure 10), this effect means that not all of the light hitting the sphere from a single focus point will emerge collimated. The change in momentum from these non-parallel rays will be less than in the ideal case, so we expect a smaller value for the restoring force.

We have both achieved trapping in two-dimensions and characterized the maximum trapping forces of the trap.

VII. Acknowledgments

I would like to thank my adviser, Dr. William E. Cooke, for his guidance, encouragement, and patience. I would also like to thank Julie Grossen and Jonathan Curley for their help and companionship in the lab. I am especially grateful for the help of Dr. Steven Smith of Harvard University with design specifics and troubleshooting. Thanks also to Thomas Nevian of Cornell University.

I would also like to thank Dr. Sharon Broadwater and Dr. Joseph Scott for their help with equipment and microscopy.

Appendix A: Photograph of Laser Tweezer Set-Up

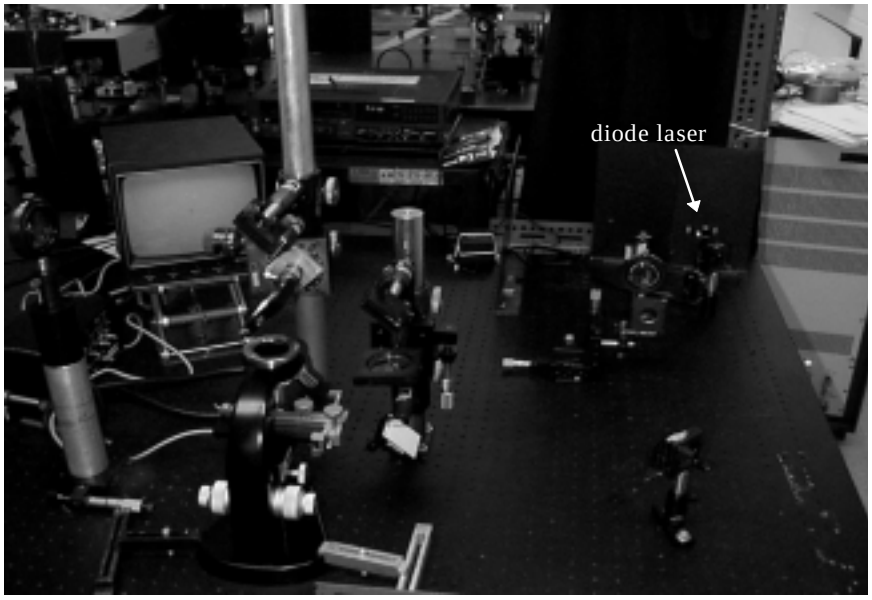

Figure 39 Digital photograph of our set-up

Appendix C: References

[1] *Star Wars*. LucasFilm, Ltd., 1977.

[2] A. Ashkin. Acceleration and trapping of particles by radiation pressure. *Phys. Rev. Lett.* **24**, 156-159 (1970).

[3] J. M. Colon, P. G. Sarosi, P. G. McGovern, A. Ashkin, J. M. Dziedzic, et. al.. Controlled micromanipulation of human sperm in three dimensions with an infrared laser optical trap: effect of sperm velocity. *Fertil. Steril.* **57**, 695-698 (1992).

[4] S. Chu. Laser Manipulation of Atoms and Particles. *Science* **252**, 861-866 (1991).

[5] K. Svoboda, and S. M. Block. Biological Application of Optical Forces. *Annu. Rev. Biophys. Biomol. Struct.* **23**, 248 (1994).

[6] A. Ashkin, *Phys. Rev. Lett.*. Atomic-beam deflection by resonance-radiation pressure. **25**, 1321-1324 (1970).

[7] A. Ashkin, *Phys. Rev. Lett.*. Trapping of atoms by resonance radiation pressure. **40**, 729-732 (1978).

[8] G. Roosen and C. Imbert. Optical levitation by means of two horizontal laser beams: a theoretical and experimental study. *Physics Letters* **59A**, 6-8 (1976).

[9] A. Ashkin and J. M. Dziedzic. Optical levitation in high vacuum. *App. Phys. Lett.* **28**, 333-335 (1976).

[10] A. Ashkin, J.M. Dziedzic, J.E. Bjorkholm, and S. Chu. Observation of a single-beam gradient trap for dielectric particles. *Optics Letters* **11**, 288-290 (1986).

[11] A. Ashkin and J.M. Dziedzic. Optical Trapping and Manipulation of Viruses and Bacteria. *Science* **235**, 1517-1520 (1987).

[12] T.N. Buican, M.J. Smyth, H.A. Crissman, G.C. Salzman, C.C. Stewart, and J.C. Martin. Automated single-cell manipulation and sorting by light trapping. *Applied Optics* **26**, 5311-5316 (1987).

[13] M.W. Berns, Y. Tadir, H. Liang, and B. Tromberg. Laser scissors and laser tweezers. In *Laser Tweezers in Cell Biology*, ed. M. P. Sheetz, 71-98, New York: Academic Press (1998).

[14] A. Ashkin. Forces of a single-beam gradient laser trap. In *Laser Tweezers in Cell Biology*, ed. M. P. Sheetz, 1-27, New York: Academic Press (1998).